

Rate of Change of Frequency Estimation for Power Systems Using Interpolated DFT and Kalman Filter

Abhinav Kumar Singh , *Member, IEEE*, and Bikash C. Pal , *Fellow, IEEE*

Abstract—This paper presents a new method for estimating the rate of change of frequency (RoCoF) of voltage or current signals measured using instrument transformers. The method is demonstrably superior to currently available methods in the literature, in terms of estimation latency and estimation error. The estimation is performed in two steps. In the first step, the analog voltage or current signal obtained from an instrument transformer is statistically processed using interpolated discrete Fourier transform (IDFT) in order to obtain the means and variances of the signal parameters. These means and variances are then given as inputs to the second step, in which Kalman filtering (KF) is used to find the final RoCoF estimate. Accurate mathematical expressions for the means and variances of signal parameters have been derived and used in the second step, which is the main reason behind the superior performance of the method. The applicability of the method has been demonstrated on a benchmark power system model.

Index Terms—Rate of change of frequency (RoCoF), statistical signal processing, discrete Fourier transform (DFT), Kalman filtering (KF), Hanning-window, instrument transformers.

NOMENCLATURE

0	denotes a zero matrix (or vector) of appropriate size.
χ	denotes a state sigma point.
γ	denotes a measurement sigma point.
A, A_c	discrete & continuous forms of state transition matrix, resp.
H	denotes measurement matrix.
I	denotes an identity matrix of appropriate size.
K	the Kalman gain matrix.
P	denotes a covariance matrix or a cross-covariance matrix.
v	column vector of process noise.
w	column vector of measurement noise.
x, y	column vectors of states and measurements, resp.
$\hat{\square}, \hat{\square}^-$	denote estimated and predicted values, resp.
λ	denotes the λ^{th} component of a DFT.
σ	denotes standard deviation, with σ^2 as variance.
θ	phase of Y 's fundamental component in rad.

f	frequency of Y 's fundamental component in Hz.
f_0	base value of f in Hz.
f_s	sampling frequency for interpolated-DFT method in Hz.
h, j	denote Hann window function, and $\sqrt{-1}$, resp.
k, \bar{k}, l	k th and $(k-1)$ th samples and the l th sigma-point, resp.
N	total samples for finding DFT.
R_f	rate of change of frequency (RoCoF) in Hz/s.
t	system time in s.
T, T_0	denote transpose and KF's sampling period (in s), resp.
W	DFT of Hann window function.
Y	denotes a sinusoidal signal with harmonics and noise.
Y_m	magnitude of Y 's fundamental component in p.u.
Z	DFT of the product of Y and h .

I. INTRODUCTION

RATE of change of frequency (RoCoF) is an important indicator for assessing the stability of energy networks and is also used as an input for protection and control devices used in power systems. RoCoF in modern energy networks is increasing as system inertia decreases due to increased integration of wind and solar energy, which are inertia-less sources of energy. RoCoF as high as ± 1 Hz/s for durations of more than 1 s have been reported by grid operators of relatively smaller grids with high penetration of wind energy, such as those of United Kingdom and Ireland [1], [2]. Grid stability challenges associated with such a high RoCoF have also been reported and studied [3]–[5].

Any control or protection scheme designed to mitigate the stability problems arising due to high RoCoF necessarily requires fast and accurate estimation of RoCoF. Inaccurate RoCoF can lead to malfunction of protection relays and limiters, and cause damage to the system. For instance, if the estimated RoCoF is lower than the actual RoCoF, then RoCoF-relays will not get triggered. However, the current limiters of automatic voltage regulators (AVRs) can get triggered due to overcurrent or undercurrent observed during a high RoCoF period. This conflicting behaviour of the two protection devices can be hazardous to the generators and the rest of the devices in the system which they are supposed to protect. Accurate estimation of RoCoF is, thus, an important necessity for safe operation of energy networks. The significance of fast and accurate estimation of RoCoF can be inferred from the fact that tripping of a RoCoF-relay played a key role in the UK power blackout of 2008 [1].

Manuscript received December 20, 2017; revised May 24, 2018 and September 18, 2018; accepted October 28, 2018. Date of publication January 31, 2019; date of current version June 18, 2019. This work was supported by the Engineering and Physical Sciences Research Council, U.K., under Grants EP/K036173/1 and EESC-P55251. Paper no. TPWRS-01892-2017. (*Corresponding author: Abhinav Kumar Singh.*)

A. K. Singh is with the School of Electronics and Computer Science, University of Southampton, Southampton SO17 1BJ, U.K. (e-mail: aks@ecs.soton.ac.uk).

B. C. Pal is with the Department of Electrical and Electronic Engineering, Imperial College London, London SW7 2AZ, U.K. (e-mail: b.pal@imperial.ac.uk).

Digital Object Identifier 10.1109/TPWRS.2018.2881151

The simplest method to estimate RoCoF is to obtain it as an average quantity. This is done by finding the change of frequency over a rolling window period, and dividing the frequency change by the duration of the window period. The problem with this method is that if RoCoF is high, then average RoCoF becomes significantly different from instantaneous RoCoF: larger the window period, larger will be the difference between average RoCoF and instantaneous RoCoF. Hence, shortest possible rolling window period should be chosen to evaluate average RoCoF in order to make it close to the instantaneous or actual RoCoF [6]. But with a shorter window period, noise or errors in measured frequency have a greater deteriorating effect on average RoCoF, rendering the estimates to be inaccurate. As noise and errors are invariably present in any measurement, an alternative solution for fast and accurate estimation of RoCoF is to use methods based on statistical signal processing, which work on the idea of filtering out noise and errors using their statistical properties.

Several methods of RoCoF estimation have been proposed in literature utilizing various techniques of statistical signal processing [7]–[19]. These techniques involve phase locked loop (PLL) ([7], [14]), Taylor-Fourier transform (TFT) and Taylor weighted least squares (TWLS) ([8], [13], [14], [16]–[19]), convolution and interpolation ([9]–[11], [15]) and Kalman filtering [12]. These papers do not focus specifically on estimation of RoCoF, instead, RoCoF is obtained as one of the parameters of synchrophasor estimation. Also, these papers do not study the relation between accuracy and latency of RoCoF estimation, or how the accuracy of estimation can be controlled. This paper aims to address this limitation, and proposes an optimal method for accurate RoCoF estimation which balances the trade-off between accuracy and latency of estimation. The novel contributions and advantages of the proposed method are enumerated as follows.

- It has been mathematically shown that it is possible for a two-step estimator to achieve a lower estimator-variance as compared to any single step estimator for RoCoF estimation.
- A two-step estimator has been proposed in which interpolated discrete Fourier transform (DFT) [20] and Kalman filtering (KF) [21] have been combined as two stages of estimation. The DFT stage dynamically provides estimates of means and variances of the inputs required by the KF stage, and this continuous updation of variances leads to noise-robustness of RoCoF estimation.
- The proposed method considers and remains accurate for varying levels of errors in measurements, from 0.1% to 10%.
- Application of Kalman filtering enables direct control of the accuracy of RoCoF estimates.
- Analytical expressions have been obtained for the means and variances of the parameter estimates of a sinusoidal signal. Most of these expressions are currently not available in literature.

Rest of the paper is organized as follows. Section II studies what type of estimator should be used for RoCoF estimation. Section III describes the process for estimation of magnitude,

phase and frequency of an analogue signal, while Section IV explains how these estimates can be further used for RoCoF estimation using KF. Section V presents simulations to demonstrate the developed estimation method. Section VI concludes the paper.

II. CHOICE OF ESTIMATOR FOR ROCOF ESTIMATION

RoCoF (R_f) can either be estimated in a single estimation step, together with the phase (θ), magnitude (Y_m) and frequency (f) of a sinusoidal signal; or it can be estimated in two steps, with phase, magnitude and frequency (or a subset of these) being estimated in the first step, and the RoCoF being estimated in the second step. In order to test which strategy of the two is a better one, Cramer Rao bounds (CRBs) have been derived in Appendices A–B. CRB gives a lower bound on the variance of any unbiased estimator [22]. If RoCoF is estimated in a single step by including it in the estimation model, then the CRBs for phase and frequency of the signal are given as follows (as derived in Appendix B).

$$\begin{aligned} \text{CRB}(\theta) &= \frac{6\sigma_Y^2}{Y_m^2} \frac{(3N^2 + 3N + 2)}{N(N-1)(N-2)} \\ \text{CRB}(f) &= \frac{24\sigma_Y^2}{Y_m^2} \left(\frac{f_s}{2\pi}\right)^2 \frac{(2N+1)(8N+11)}{N(N^2-1)(N^2-4)} \end{aligned} \quad (1)$$

Here σ_Y^2 is the variance of the noise in the sinusoidal signal, N is the total number of samples used for finding the estimates and f_s is the sampling frequency. Alternatively, if RoCoF is estimated in two steps by not including it in the estimation model for the first step, then the CRBs for phase and frequency of the signal are given as follows (as derived in Appendix A).

$$\begin{aligned} \text{CRB}(\theta) &= \frac{4\sigma_Y^2}{Y_m^2} \frac{(2N+1)}{N(N-1)} \\ \text{CRB}(f) &= \frac{24\sigma_Y^2}{Y_m^2 N(N^2-1)} \left(\frac{f_s}{2\pi}\right)^2 \end{aligned} \quad (2)$$

It can be inferred from (1), (2) that for given σ_Y^2 , N and f_s , and for large N (that is, $N \gg 1$), $\text{CRB}(\theta)$ for one-step estimation strategy is approximately 9/4 times larger than $\text{CRB}(\theta)$ for two-step estimation strategy. Similarly, $\text{CRB}(f)$ for one-step estimation is approximately 16 times larger than $\text{CRB}(f)$ for two-step estimation. This shows that if RoCoF is included in estimation model, then the CRBs for phase and frequency estimation are always larger than when RoCoF is not included in the estimation model. Thus, it is better to first estimate phase and frequency, and then use their means and variances in a second step to estimate RoCoF, as two-step estimation of RoCoF can achieve lower variance for estimates than single step estimation. Also, as RoCoF is related to phase and frequency using a simple linear and dynamic model, Kalman filter can be used to dynamically estimate RoCoF if the means and variances of phase and frequency are already known. This is the rationale behind using a two-step estimator, in which the first step provides accurate estimates of means and variances of phase and frequency of a sinusoidal signal, and the second step dynamically provides

RoCoF estimation using KF. The next two sections provide the details of the two steps of estimation.

III. STEP 1: INTERPOLATED DFT BASED ESTIMATION

Several methods have been proposed in literature for estimating the parameters of a sinusoidal signal, but most of these methods are computationally expensive and, hence, are not suitable for real-time applications [23]. Recently, an interpolated DFT based estimation method was proposed in [20] and was shown to be both fast and accurate enough for real-time control applications in power systems. This method has been further developed in this section for finding the estimates of frequency, magnitude and phase of the fundamental components of measurements obtained from CTs and VTs.

The k th sample of an analogue signal $Y(t)$, sampled at a frequency f_s , can be denoted by $Y_k = Y_m \sin\left(\frac{2\pi kf}{f_s} + \theta\right) + \epsilon$, where $Y_m \sin\left(\frac{2\pi kf}{f_s} + \theta\right)$ is the fundamental component of the signal, while ϵ denotes other harmonics and high-frequency components in the signal. The fundamental component of the signal can be extracted by multiplying the samples of the analogue signal with a suitable window function which eliminates other harmonics and high-frequency components in the signal, followed by finding its DFT. One such function is Hanning window function given by $h_k = \sin^2\left(\frac{\pi k}{N}\right)$, and if this function is multiplied with N samples of Y_k , the DFT of the product is given by $Z(\lambda)$ as follows [20].

$$\begin{aligned} Z(\lambda) &= \sum_{k=0}^{N-1} Y_k h_k e^{-j2\pi k\lambda} \\ &= \frac{Y_m}{2j} e^{j\theta} W\left(\lambda - \frac{fN}{f_s}\right) - \frac{Y_m}{2j} e^{-j\theta} W\left(\lambda + \frac{fN}{f_s}\right) \end{aligned} \quad (3)$$

where, Y_m , θ and f are magnitude, phase and frequency of Y 's fundamental component, respectively; $\lambda \in \{0, 1, \dots, N-1\}$; and $W(\lambda)$ is the following DFT of Hanning window function.

$$W(\lambda) = \sum_{k=0}^{N-1} h_k e^{-j2\pi k\lambda} = \sum_{k=0}^{N-1} \sin^2\left(\frac{\pi k}{N}\right) e^{-j2\pi k\lambda} \quad (4)$$

The key concept in interpolated-DFT based estimation is to approximate $W(\lambda)$ with the following expression, provided that $N \gg 1$ and $\lambda \ll N$ [20], [24].

$$W(\lambda) \approx \frac{N}{4\pi j} \frac{(1 - e^{-j2\pi\lambda})}{(\lambda - \lambda^3)} \quad (5)$$

By substituting (5) in (3), $Z(\lambda)$ can be expressed as follows for $N \gg 1$ and $\lambda \ll N$.

$$\begin{aligned} Z_\lambda = Z(\lambda) &= \frac{\hat{Y}_m N}{8\pi} \left[\frac{e^{j\hat{\theta}} (e^{-j2\pi(\lambda - \frac{\hat{f}N}{f_s})} - 1)}{(\lambda - \frac{\hat{f}N}{f_s}) - (\lambda - \frac{\hat{f}N}{f_s})^3} \right. \\ &\quad \left. - \frac{e^{-j\hat{\theta}} (e^{-j2\pi(\lambda + \frac{\hat{f}N}{f_s})} - 1)}{(\lambda + \frac{\hat{f}N}{f_s}) - (\lambda + \frac{\hat{f}N}{f_s})^3} \right] \end{aligned} \quad (6)$$

where \hat{Y}_m , $\hat{\theta}$ and \hat{f} denote the estimates of Y_m , θ and f , respectively. As (6) has three unknowns (which are \hat{Y}_m , $\hat{\theta}$ and \hat{f}), three distinct equations are required to estimate these unknowns. This can be done by choosing any three distinct values of λ in (6) (say $\lambda = 1$, $\lambda = 2$ and $\lambda = 3$). The obtained values of \hat{Y}_m , $\hat{\theta}$ and \hat{f} will have associated estimation errors which will depend on N and on the values of λ which are used for generating the three distinct equations. More precisely, these estimation errors are inversely proportional to N^4 [20], and, hence, N should be as large as practically feasible. In this paper N is taken to be in the order of 10^3 , as this is the highest order for N for which interpolated-DFT can run on a state-of-the-art DSP processor without overloading it [20]. Also, for a given N , the estimation errors are minimized if the choices for λ are taken as $\lambda = 0$, $\lambda = 1$ and $\lambda = 2$, provided that $\frac{\hat{f}N}{f_s} < 2.1$; otherwise, for $2.1 < \frac{\hat{f}N}{f_s} < 3$, the errors are minimized if the choices are $\lambda = 1$, $\lambda = 2$ and $\lambda = 3$ [20]. The value of $\frac{\hat{f}N}{f_s}$ should not be greater than 3 as then the latency in obtaining the estimated values becomes too large, and at the same time it should not be too small as then the accuracy of estimation is diminished [20]. In this paper an intermediate value of $\frac{\hat{f}N}{f_s} \approx 1.5$ has been taken and, hence, the former choices of $\lambda = 0$, $\lambda = 1$ and $\lambda = 2$ are applicable.

Remark 1: $\frac{\hat{f}N}{f_s}$ is an unknown quantity as f needs to be estimated. But because of power system operational requirements [25], f should remain within 5% of the base system frequency, f_0 (which is usually 50 Hz or 60 Hz), and, hence, if N and f_s are chosen such that $\frac{f_0 N}{f_s} = 1.5$, then $\frac{\hat{f}N}{f_s} \approx 1.5$.

The 3 equations which are obtained by putting $\lambda = 0$, $\lambda = 1$ and $\lambda = 2$ in (6) can be written in matrix form as follows.

$$\begin{bmatrix} \frac{\hat{f}N}{f_s} - 2 & \frac{\hat{f}N}{f_s} + 2 & Z_0 \\ \frac{\hat{f}N}{f_s} + 1 & \frac{\hat{f}N}{f_s} - 1 & Z_1 \\ 1 & 1 & Z_2 \\ \frac{\hat{f}N}{f_s} & \frac{\hat{f}N}{f_s} & Z_2 \\ \frac{\hat{f}N}{f_s} - 3 & \frac{\hat{f}N}{f_s} + 3 & Z_2 \end{bmatrix} \begin{bmatrix} \frac{\hat{Y}_m N e^{j\hat{\theta}} (e^{j2\pi \frac{\hat{f}N}{f_s} - 1})}{8\pi \frac{\hat{f}N}{f_s} (\frac{\hat{f}N}{f_s} - 1) (\frac{\hat{f}N}{f_s} - 2)} \\ \frac{\hat{Y}_m N e^{-j\hat{\theta}} (e^{-j2\pi \frac{\hat{f}N}{f_s} - 1})}{8\pi \frac{\hat{f}N}{f_s} (\frac{\hat{f}N}{f_s} + 1) (\frac{\hat{f}N}{f_s} + 2)} \\ -1 \end{bmatrix} = \begin{bmatrix} 0 \\ 0 \\ 0 \end{bmatrix} \quad (7)$$

Equation (7) implies that the product of a square-matrix and a column vector is equal to a zero vector, when both the matrix and the vector have non-zero elements. This can only happen if the columns of the matrix are linearly dependent, that is, the determinant of the matrix is zero, given as follows.

$$\begin{vmatrix} \frac{\hat{f}N - 2f_s}{\hat{f}N + f_s} & \frac{\hat{f}N + 2f_s}{\hat{f}N - f_s} & Z_0 \\ 1 & 1 & Z_1 \\ \frac{\hat{f}N}{\hat{f}N - 3f_s} & \frac{\hat{f}N}{\hat{f}N + 3f_s} & Z_2 \end{vmatrix} = 0 \quad (8)$$

Simplification of the above determinant gives \hat{f} as follows.

$$\hat{f} = \frac{f_s}{N} \sqrt{\frac{Z_0 + 2Z_1 + 9Z_2}{Z_0 - 2Z_1 + Z_2}} \quad (9)$$

$\hat{\theta}$ can be obtained by substituting the above value of \hat{f} back into (6) and eliminating \hat{Y}_m . To do this, the equation which

is obtained by putting $\lambda = 0$ in (6) is divided by the equation obtained by putting $\lambda = 1$ in (6), which comes as follows.

$$\begin{aligned} \frac{Z_0}{Z_1} &= \frac{e^{j\hat{\theta}}B + e^{-j\hat{\theta}}C}{e^{j\hat{\theta}}E + e^{-j\hat{\theta}}F}; \quad B = \frac{1 - e^{-\frac{j2\pi\hat{f}N}{f_s}}}{\frac{\hat{f}N}{f_s} - \left[\frac{\hat{f}N}{f_s}\right]^3}, \\ C &= \frac{1 - e^{-\frac{j2\pi\hat{f}N}{f_s}}}{\frac{\hat{f}N}{f_s} - \left[\frac{\hat{f}N}{f_s}\right]^3}, \\ E &= \frac{1 - e^{-\frac{j2\pi\hat{f}N}{f_s}}}{\frac{\hat{f}N}{f_s} - 1 - \left[\frac{\hat{f}N}{f_s} - 1\right]^3}, \\ F &= \frac{1 - e^{-\frac{j2\pi\hat{f}N}{f_s}}}{\frac{\hat{f}N}{f_s} + 1 - \left[\frac{\hat{f}N}{f_s} + 1\right]^3} \end{aligned} \quad (10)$$

Solving for $e^{j\hat{\theta}}$ using (10) gives the following expression.

$$e^{j\hat{\theta}} = \sqrt{\frac{Z_0F - Z_1C}{Z_1B - Z_0E}} \Rightarrow \hat{\theta} = \frac{1}{2j} \ln \left\{ \frac{Z_0F - Z_1C}{Z_1B - Z_0E} \right\} \quad (11)$$

Using (11) and (6) (with $\lambda = 0$), \hat{Y}_m comes as follows.

$$\hat{Y}_m = 8\pi Z_0 / \left[N \left\{ B e^{j\hat{\theta}} + C e^{-j\hat{\theta}} \right\} \right] \quad (12)$$

where B , C , and $e^{j\hat{\theta}}$ are given by (10), (11).

Remark 2: It should be noted that \hat{f} , $\hat{\theta}$ and \hat{Y}_m are real quantities, but they are obtained as functions of complex quantities (given in the right hand sides (RHSs) of (9), (11) and (12), respectively). Hence, these quantities will have negligible but finite imaginary parts associated with them because of finite computational accuracy of any computational device. This fact can be further understood using a simple example. Suppose the real and imaginary parts of $e^{i\pi}$ need to be computed. From basic maths, it is known that real part of $e^{i\pi}$ is $\cos \pi = -1$, and its imaginary part is $\sin \pi = 0$. But, as π is an irrational number, any computer stores only an approximate value for π , with finite number of digits after decimal. The computer uses this stored value of π for calculating the real and imaginary parts of $e^{i\pi}$. If the value stored for π in the computer is $(\pi - \epsilon)$, where ϵ is the difference between the actual value of π and the stored value of π , then the value which is computed for the imaginary part of $e^{i\pi}$ is equal to $\sin(\pi - \epsilon) \approx \epsilon$. Thus, the imaginary part computed for $e^{i\pi}$ is non-zero, and it is approximately equal to a small number ϵ , which corresponds to the computational accuracy of the computer. This fact can be easily verified by evaluating the expression $\text{imag}(\exp(i*\pi))$ in MATLAB (or a similar expression in any other programming software). Just as the actual imaginary part of $e^{i\pi}$ is zero, in the same way, the actual values of \hat{f} , $\hat{\theta}$ or \hat{Y}_m should have zero imaginary parts. This is because \hat{f} , $\hat{\theta}$ or \hat{Y}_m denote real quantities, and their mathematical expressions will also be purely real, as these expressions have been derived by applying principles of maths on equation (7). Thus, during implementation, the imaginary parts should be ignored and only the real parts of RHSs of (9),

(11) and (12) should be assigned to \hat{f} , $\hat{\theta}$ or \hat{Y}_m , respectively. Also, as \hat{f} and \hat{Y}_m are strictly positive, absolute values of real parts of respective RHSs should be assigned to them. Moreover, as by definition $\hat{\theta}$ lies in the interval $(-\pi/2, \pi/2]$, hence, it should be ‘unwrapped’ by adding or subtracting suitable multiples of π .

It was found in [20] that the variance of the above estimate of \hat{f} in (9) is approximately twice the minimum possible variance which is theoretically achievable using any unbiased estimator (known as Cramer-Rao bound (CRB) [26]). CRB for frequency estimation of a sinusoidal signal has been derived in [26] (and also in Appendix A) and is given by $\text{CRB}(\hat{f})$ (in Hz^2) as follows.

$$\text{CRB}(\hat{f}) = \left(\frac{f_s}{2\pi} \right)^2 \frac{24\sigma_Y^2}{\hat{Y}_m^2 N(N^2 - 1)} \quad (13)$$

Here σ_Y^2 is the p.u. noise variance of Y . CRBs for variances of \hat{Y}_m and $\hat{\theta}$, and cross-variance of $\hat{\theta}$ and \hat{f} have been derived in Appendix A (and not in [26]), and are given by $\text{CRB}(\hat{Y}_m)$ (in p.u.), $\text{CRB}(\hat{\theta})$ (in rad^2) and $\text{CRB}(\hat{\theta}, \hat{f})$ (in rad/s), respectively, as follows.

$$\begin{aligned} \text{CRB}(\hat{Y}_m) &= \frac{2\sigma_Y^2}{N}; \quad \text{CRB}(\hat{\theta}) = \frac{4\sigma_Y^2(2N+1)}{\hat{Y}_m^2 N(N-1)} \\ \text{CRB}(\hat{\theta}, \hat{f}) &= \frac{-12\sigma_Y^2}{Y_m^2 N(N-1)} \frac{f_s}{2\pi} \end{aligned} \quad (14)$$

Following the statistical analysis given in [20] for finding the variance of \hat{f} , the variances of \hat{f} , \hat{Y}_m and $\hat{\theta}$, and cross-variance of $\hat{\theta}$ and \hat{f} are found to be approximately two, two, six and two times the above CRBs in (14), respectively; and hence, the estimated variances of \hat{f} , $\hat{\theta}$ and \hat{Y}_m , and estimated cross-variance of $\hat{\theta}$ and \hat{f} are given by $\hat{\sigma}_f^2$ (in p.u.), $\hat{\sigma}_{Y_m}^2$ (in p.u.), $\hat{\sigma}_\theta^2$ (in rad^2) and $\hat{\sigma}_{\theta f}$ (in rad), respectively, as follows.

$$\begin{aligned} \hat{\sigma}_f^2 &= 2 \times \text{CRB}(\hat{f})/f_0^2; \quad \hat{\sigma}_{Y_m}^2 = 2 \times \text{CRB}(\hat{Y}_m); \\ \hat{\sigma}_\theta^2 &= 6 \times \text{CRB}(\hat{\theta}); \quad \hat{\sigma}_{\theta f} = 2 \times \text{CRB}(\hat{\theta}, \hat{f})/f_0 \end{aligned} \quad (15)$$

where $\text{CRB}(\hat{f})$, $\text{CRB}(\hat{Y}_m)$, $\text{CRB}(\hat{\theta})$ and $\text{CRB}(\hat{\theta}, \hat{f})$ are given by (13)–(14). Estimates obtained above are given as inputs to the Kalman filtering stage, as detailed in the next section.

Remark 3: The advantage of obtaining the analytical expressions for $\hat{\sigma}_f^2$, $\hat{\sigma}_\theta^2$ and $\hat{\sigma}_{\theta f}$ in (13)–(15) is that these estimates of variances and cross variance can be continuously updated and provided to the Kalman filtering stage, along with \hat{f} and $\hat{\theta}$, thereby improving the accuracy of RoCoF estimation.

IV. STEP 2: KALMAN FILTERING

Kalman filtering is a recursive method for obtaining state estimates of a dynamic system. As a simple and linear dynamic model defines RoCoF in terms of phase and frequency of an analog signal, any variant of Kalman filter can be used to estimate RoCoF. In this paper unscented KF (UKF [21]) has been used for performing RoCoF estimation using the parameter estimates obtained from the interpolated DFT (IDFT) stage.

The process model used for estimating RoCoF is given as follows.

$$\dot{\mathbf{x}} = \mathbf{A}_c \mathbf{x} + \mathbf{v}, \quad \text{and}, \quad \mathbf{x} = \begin{bmatrix} \theta \\ f \\ R_f \end{bmatrix}; \quad \mathbf{A}_c = \begin{bmatrix} 0 & 2\pi & 0 \\ 0 & 0 & 1 \\ 0 & 0 & 0 \end{bmatrix} \quad (16)$$

KF is a discrete method and, hence, the process model given by (16) needs to be discretized before KF can be applied to it. Discretizing (16) at a sampling period T_0 , by using zero order hold (ZOH) approximation [27], gives the following equation (where k and \bar{k} represent the k^{th} and $(k-1)^{\text{th}}$ samples, respectively).

$$\mathbf{x}^k = \mathbf{A} \mathbf{x}^{\bar{k}} + \mathbf{v}^{\bar{k}}; \quad \text{and} \quad \mathbf{A} = e^{T_0 \mathbf{A}_c} = \begin{bmatrix} 1 & 2\pi T_0 & \pi T_0^2 \\ 0 & 1 & T_0 \\ 0 & 0 & 1 \end{bmatrix} \quad (17)$$

$\mathbf{v}^{\bar{k}}$ in the above process model is the process-noise with zero mean and associated covariance matrix denoted by \mathbf{P}_v . As θ and f are measured quantities for the KF stage and only have associated measurement noises, the process-noise variances and cross-variances associated with θ and f are all zero. But the process-noise variance associated with the RoCoF is not zero. Denoting this variance by $\sigma_{R_f}^2$ (in p.u./s², and is equal to $f_0^2 \sigma_{R_f}^2$ in Hz²/s²), the process-noise model is given as follows.

$$\mathbf{v}^k = \begin{bmatrix} v_{\theta k} \\ v_{f k} \\ v_{R_f k} \end{bmatrix}; \quad \hat{\mathbf{v}}^k = \begin{bmatrix} 0 \\ 0 \\ 0 \end{bmatrix}; \quad \mathbf{P}_v = \begin{bmatrix} 0 & 0 & 0 \\ 0 & 0 & 0 \\ 0 & 0 & f_0^2 \sigma_{R_f}^2 \end{bmatrix} \quad (18)$$

Remark 4: The parameter $\sigma_{R_f}^2$ in the above process-noise model is the only non-zero term of \mathbf{P}_v and it corresponds to the expected variance of the noise in RoCoF estimates. Hence, $\sigma_{R_f}^2$ directly controls the accuracy of RoCoF estimation. This has been further explained and demonstrated in Section V-B.

Kalman filter also requires a measurement model besides a process model. The estimates of phase, θ^k (defined by (10), (11) and denoted by $\hat{\theta}^k$), and of frequency, f^k (defined by (9) and denoted by \hat{f}^k), which are obtained in the IDFT stage, are used as measurements for the UKF stage. After incorporating the measurement noise, \mathbf{w}^k , the measurement model is given as follows.

$$\mathbf{y}^k = \begin{bmatrix} \hat{\theta}^k \\ \hat{f}^k \end{bmatrix} = \begin{bmatrix} \theta^k \\ f^k \end{bmatrix} + \mathbf{w}^k \Rightarrow \mathbf{y}^k = \mathbf{H} \mathbf{x}^k + \mathbf{w}^k$$

where, $\mathbf{H} = \begin{bmatrix} 1 & 0 & 0 \\ 0 & 1 & 0 \end{bmatrix}$ (19)

\mathbf{y}^k in the above measurement model consists of estimated quantities which have finite measurement-noises. These noises are denoted by \mathbf{w}^k in the measurement model, and associated

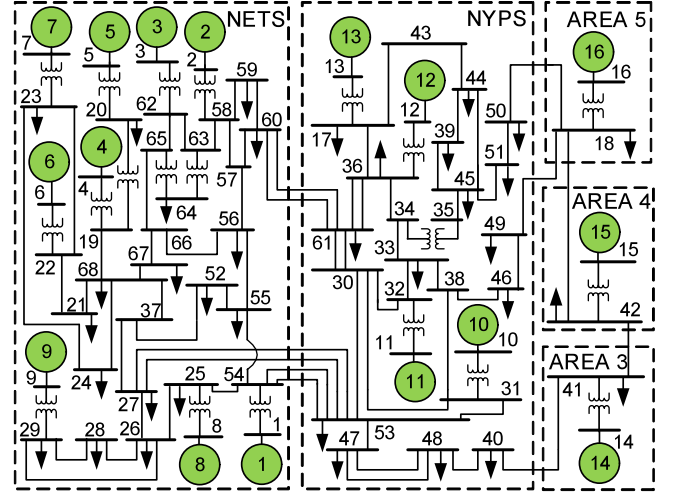


Fig. 1. Line diagram of the 16-machine, 68-bus, power system model.

mean and variance are defined as follows.

$$\mathbf{w}^k = \begin{bmatrix} w_{\theta k} \\ w_{f k} \end{bmatrix}; \quad \hat{\mathbf{w}}^k = \begin{bmatrix} 0 \\ 0 \end{bmatrix}; \quad \mathbf{P}_w = \begin{bmatrix} \hat{\sigma}_{\theta}^2 & f_0 \hat{\sigma}_{\theta f k} \\ f_0 \hat{\sigma}_{\theta f k} & f_0^2 \hat{\sigma}_{f k}^2 \end{bmatrix} \quad (20)$$

Thus, the two quantities which are required by the UKF stage from the IDFT stage are \mathbf{y}^k and \mathbf{P}_w^k , given by (19)–(20) and (9)–(15). These quantities should be updated every T_0 s, which is the sampling period of the UKF stage. With (16)–(20) as model, the filtering equations of UKF for k^{th} sample are given as follows [28].

STEP 1: Initialize

if ($k=1$) then initialize $\hat{\mathbf{x}}^k = \mathbf{x}^0 = [0 \ 1 \ 0]^T$, $\mathbf{P}_x^k = \mathbf{P}_v$.

STEP 2: Generate sigma points

$$\chi_l^k = \hat{\mathbf{x}}^k + \left(\sqrt{3\mathbf{P}_x^k} \right)_l, \quad l = 1, 2, 3;$$

$$\chi_l^k = \hat{\mathbf{x}}^k - \left(\sqrt{3\mathbf{P}_x^k} \right)_l, \quad l = 4, 5, 6$$

STEP 3: Predict states

$$\chi_l^{k-} = \mathbf{A} \chi_l^k; \quad \hat{\mathbf{x}}^{k-} = \frac{1}{6} \sum_{l=1}^6 \chi_l^{k-}$$

$$\mathbf{P}_x^{k-} = \frac{1}{6} \sum_{l=1}^6 [\chi_l^{k-} - \hat{\mathbf{x}}^{k-}] [\chi_l^{k-} - \hat{\mathbf{x}}^{k-}]^T + \mathbf{P}_v$$

STEP 4: Predict measurements

$$\gamma_l^{k-} = \mathbf{H} \chi_l^k; \quad \hat{\mathbf{y}}^{k-} = \frac{1}{6} \sum_{l=1}^6 \gamma_l^{k-}$$

$$\mathbf{P}_y^{k-} = \frac{1}{6} \sum_{l=1}^6 [\gamma_l^{k-} - \hat{\mathbf{y}}^{k-}] [\gamma_l^{k-} - \hat{\mathbf{y}}^{k-}]^T + \mathbf{P}_w^k$$

$$\mathbf{P}_{xy}^{k-} = \frac{1}{6} \sum_{l=1}^6 [\chi_l^{k-} - \hat{\mathbf{x}}^{k-}] [\gamma_l^{k-} - \hat{\mathbf{y}}^{k-}]^T$$

STEP 5: Kalman update

$$\mathbf{K}^k = \mathbf{P}_{xy}^{k-} (\mathbf{P}_y^{k-})^{-1}; \quad \hat{\mathbf{x}}^k = \hat{\mathbf{x}}^{k-} + \mathbf{K}^k (\mathbf{y}^k - \hat{\mathbf{y}}^{k-})$$

$$\mathbf{P}_x^k = \mathbf{P}_x^{k-} - \mathbf{K}^k [\mathbf{P}_{xy}^{k-}]^T$$

STEP 6: Output and time update

output $\hat{\mathbf{x}}^k$ and \mathbf{P}_x^k , $k \leftarrow (k+1)$, goto STEP 1.

V. CASE STUDY

A model 16-machine, 68-bus benchmark test system (Fig. 1) has been used for the case study and MATLAB-Simulink has

been used for its modelling and simulation. A detailed description of the system is given in [29], [30] or [31].

The RoCoF of the terminal voltage of each generation unit in the system is obtained dynamically using the proposed IDFT-UKF RoCoF estimator. The measurement which is required by the estimator is the terminal voltage of a generation unit, $V(t)$, and is generated by adding noise to the simulated analogue values of terminal voltage the unit. As mentioned in IEEE and IEC standards ([35], [36]), the measurement error in industrial CTs and VTs lies in the range of 0.1%–3%. In this case study, an intermediate value has been taken for the variance of noise in $V(t)$, and it is set as 1%, that is, $\sigma_V^2 = 0.01^2$ (p.u.). Also, as explained in Section III, N , f_0 and f_s are taken as 1200, 50 Hz and 40000 Hz, respectively. The sampling period of UKF stage, T_0 , is taken as 0.01 s, as explained in [29], [28] or [32]; and thus, the estimates obtained from the IDFT stage are also updated every 0.01 s. Also, $\sigma_{R_f}^2 = 1 \times 10^{-7}$ (p.u./s²) in (18). The estimation results of the proposed method have also been compared with currently available methods. Due to limitation of space, results of only selected methods have been shown in this case study, and these methods include: 1) the rolling window averaging method (or $\Delta f/\Delta t$ method), 2) a standard PMU based method as given in [19], and 3) the method given in [13], which is one of the currently best available methods in literature in terms of accuracy and estimation-latency.

Estimation latency refers to the total interval between the time at which a physical quantity takes a certain value, and the time at which this value of the physical quantity gets estimated. In the case study, estimation latency translates to the interval between the time at which a simulated value of RoCoF arrives, and the time at which this value of RoCoF is estimated by an estimator using some measurable quantity (or quantities) as input (which is analog voltage signal in this case).

The system starts from a steady state in the simulation. Then at $t = 1$ s, a disturbance is created by a three-phase fault at bus 54 and is cleared after 0.18 s by opening of one of the tie-lines between buses 53–54. This creates a RoCoF event in which the system RoCoF touches around ± 1 Hz/s for a few seconds. The simulated RoCoF along with its estimated values for one of the units (the 13th generation unit) have been plotted in Fig. 2 for the four RoCoF estimation methods. The parameters of the estimators have been selected in such a way that the estimation latencies for all the methods remain same and are equal to 110 ms.

A. Estimation Accuracy

It can be observed from Fig. 2 that the estimation performance of the bottom two methods is comparable, and is far superior than the top two methods. As it is not clear from Fig. 2 whether the proposed IDFT-UKF method performs better than the GTWLS-IDFT method, both of these methods have been plotted together in Fig. 3, along with the plots of corresponding squared estimation errors.

It can be seen in Fig. 3 that the estimation provided by the proposed IDFT-UKF method is relatively ‘smoother’ than the GTWLS-IDFT method, that is, the estimation errors are closer

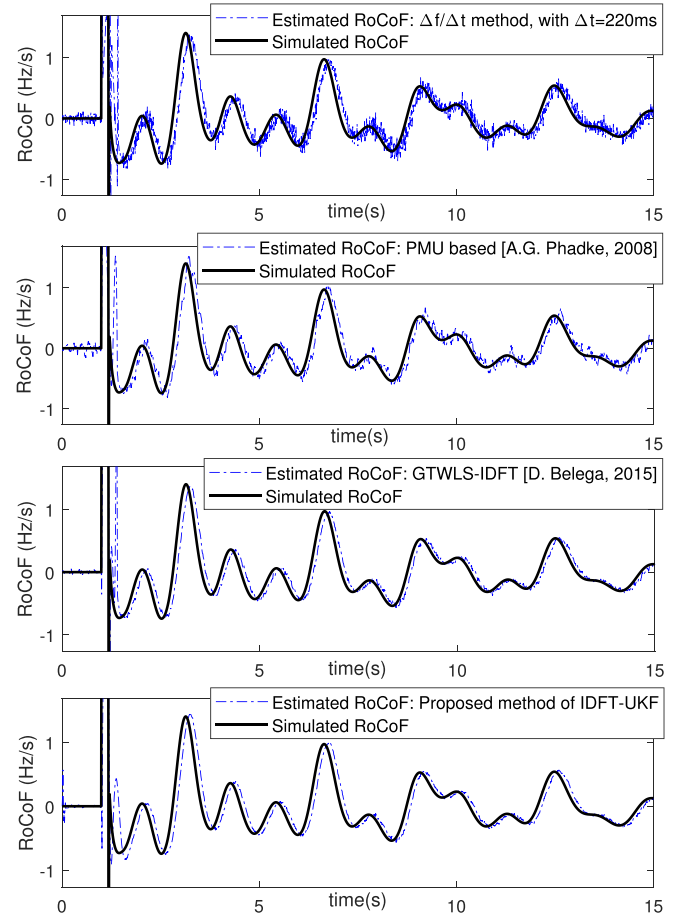


Fig. 2. Comparison of RoCoF estimation for the 13th unit for estimation latency of 110 ms.

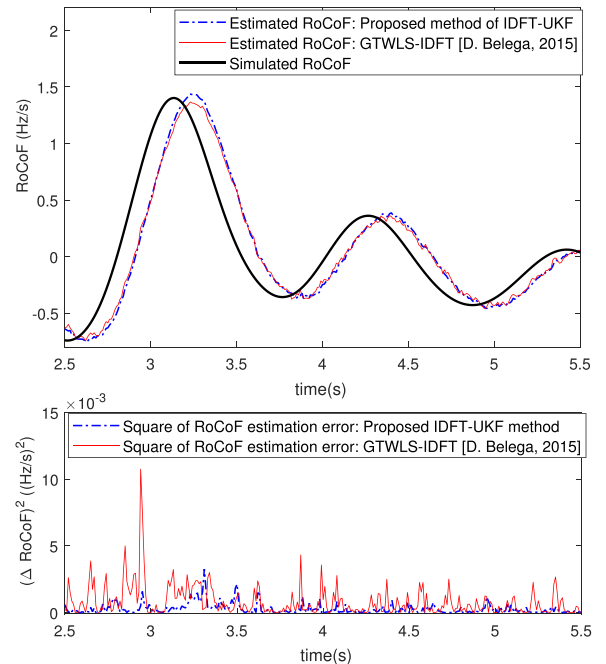


Fig. 3. Detailed comparison of estimation performance for GTWLS-IDFT and IDFT-UKF methods.

TABLE I
RoCoF ESTIMATION ERRORS FOR ESTIMATION LATENCY OF 110 ms

Estimation method	Maximum error (Hz/s)	Root mean square error (Hz/s)
$\Delta f/\Delta t$ method, $\Delta t = 220\text{ms}$	0.30	8.5×10^{-2}
PMU based method [19]	0.26	7.2×10^{-2}
GTWLS-IDFT based method [13]	0.10	2.5×10^{-2}
IDFT-UKF based proposed method	0.05	1.5×10^{-2}

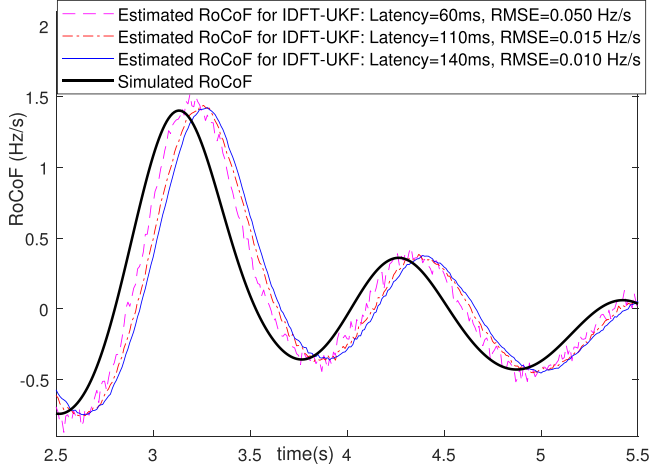


Fig. 4. Dependence of estimation latency on RMSE.

to zero and the maximum estimation error is much lower. To be precise, the root mean square errors (RMSEs) and the maximum errors for the four methods have been tabulated in Table I for estimation latency of 110ms. It can be inferred from Table I that both the RMSE and the maximum error for the proposed method remain around three-fifth of those for the GTWLS-IDFT method. In fact, the proposed method satisfies all the IEEE standard limits for RoCoF estimation as specified in [33], [34]. These limits are: maximum error of 0.10 Hz/s, RMSE of 2×10^{-2} Hz/s and corresponding maximum estimation latency of 120 ms.

B. Controlling RMSE and Its Effect on Estimation Latency

It was briefly mentioned in Section IV that $\sigma_{R_f}^2$ is the process-noise variance (in p.u./s²) associated with the RoCoF, and as it is the only non-zero term of \mathbf{P}_v as given in (18), $\sigma_{R_f}^2$ directly controls the variance of the estimated RoCoF. Hence, if $\sigma_{R_f}^2$ is set equal to 1×10^{-7} (p.u./s²), then the standard deviation or RMSE of the estimated RoCoF is expected to be around $\sqrt{1 \times 10^{-7}}$ (p.u./s) or $\sqrt{1 \times 10^{-7}} \times f_0 = \sqrt{1 \times 10^{-7}} \times 50 \approx 1.5 \times 10^{-2}$ (Hz/s), which is what is observed in Table I.

Estimation latency depends on both σ_Y^2 (noise variance of the input signal) and $\sigma_{R_f}^2$. Fig. 4 shows how estimation latencies vary with RMSEs for a fixed $\sigma_Y^2 = 0.01^2$ (p.u.) for the proposed method. It can be observed from the figure that latency is low for high RMSEs, and latency increases with decrease in RMSE. This is expected as the UKF estimator requires longer time to achieve smaller RMSE in the estimated RoCoF. Thus, for a given noise level of input signal, a desired level of estimation RMSE can be directly obtained, and such a control over accuracy of

estimates can be beneficial in accuracy sensitive applications. Also, for latency sensitive applications a given level of latency can be obtained indirectly by assigning a suitable value to $\sigma_{R_f}^2$. In any case, as only one parameter, $\sigma_{R_f}^2$, decides both RMSE and latency, it can be easily manipulated as per the application, or to achieve balance in accuracy and latency.

Remark 5: It should be noted here that $\sigma_{R_f}^2$ should not be set as zero, or to infinitesimal values, as this would produce incorrect estimation results from UKF – no estimator can provide infinite accuracy of estimation. This limiting value of $\sigma_{R_f}^2$, below which incorrect estimation results are obtained, depends on noise variance of input signal, and can be obtained using trial-and-error. In the case study, it is found that for an input noise variance of $\sigma_Y^2 = 0.01^2$ (p.u.), the limiting value of $\sigma_{R_f}^2$ comes out to be 1×10^{-9} (p.u./s²).

C. Computational Feasibility

Computational feasibility of the proposed method can be inferred from the fact that the entire simulation, including simulation of the power system, with the four estimators at each machine, runs in faster-than-real-time on a personal computer with Intel Core 2 Duo, 2.0 GHz CPU and 2 GB RAM. The expression ‘faster-than-real-time’ here means that 1 second of the simulation takes less than 1 second of processing time. Thus, the method can be easily implemented using current technologies.

VI. CONCLUSION

A two-stage method for dynamic RoCoF estimation in power systems has been proposed which can provide RoCoF estimates of analogue signals of voltage or current measured using instrument transformers. The proposed method provides better accuracy for a given estimation latency as compared to currently available methods. The proposed method also provides direct control over the accuracy of estimation, and can be easily tweaked to suit any kind of application and to strike a balance between accuracy and estimation latency.

APPENDIX A

DERIVATION OF CRAMER RAO BOUND (CRB) FOR PARAMETER ESTIMATION OF A SINUSOIDAL SIGNAL

Let the N samples of a sinusoidal signal Y , sampled at a sampling frequency of f_s , be given as follows.

$$Y_k = Y_m \sin \phi_k + \epsilon_k, \quad \phi_k = \frac{2\pi k f}{f_s} + \theta, \quad \forall k = 1, 2, \dots, N \quad (21)$$

Here, ϵ_k is the noise in Y_k , and the variance of ϵ_k is σ_Y^2 . The set of parameters which need to be estimated for (21) is $\Theta = \{\Theta_1, \Theta_2, \Theta_3\} = \{Y_m, \theta, f\}$. A lower bound on the variance of any unbiased estimator of Θ is given by the CRB [22], which is found using the inverse of the information matrix, $\mathbb{I}(\Theta)$. For (21), the (i, j) th element of the matrix $\mathbb{I}(\Theta)$ is given as follows.

$$\mathbb{I}_{i,j}(\Theta) = \frac{1}{\sigma_Y^2} \sum_{k=1}^N \frac{\partial Y_k}{\partial \Theta_i} \frac{\partial Y_k}{\partial \Theta_j} \quad (22)$$

After evaluating the partial derivatives in (22) using (21), various elements of $\mathbb{I}(\Theta)$ are given as follows.

$$\begin{aligned}\mathbb{I}_{1,1}(\Theta) &= \frac{1}{2\sigma_Y^2} \sum_{k=1}^N (1 - \cos(2\phi_k)) \\ \mathbb{I}_{1,2}(\Theta) = \mathbb{I}_{2,1}(\Theta) &= \frac{Y_m}{2\sigma_Y^2} \sum_{k=1}^N \sin(2\phi_k) \\ \mathbb{I}_{1,3}(\Theta) = \mathbb{I}_{3,1}(\Theta) &= \frac{Y_m}{2\sigma_Y^2} \sum_{k=1}^N \frac{2\pi k}{f_s} \sin(2\phi_k) \\ \mathbb{I}_{2,2}(\Theta) &= \frac{Y_m^2}{2\sigma_Y^2} \sum_{k=1}^N (1 + \cos(2\phi_k)) \\ \mathbb{I}_{2,3}(\Theta) = \mathbb{I}_{3,2}(\Theta) &= \frac{Y_m^2}{2\sigma_Y^2} \sum_{k=1}^N \frac{2\pi k}{f_s} (1 + \cos(2\phi_k)) \\ \mathbb{I}_{3,3}(\Theta) &= \frac{Y_m^2}{2\sigma_Y^2} \sum_{k=1}^N \left(\frac{2\pi k}{f_s}\right)^2 (1 + \cos(2\phi_k))\end{aligned}$$

where, $\phi_k = \frac{2\pi k f}{f_s} + \theta$ (23)

Since $N \gg 1$ and $f \ll f_s$, as explained in Section III, the above elements of $\mathbb{I}(\Theta)$ get simplified to the following expressions using basic rules of summation of trigonometric series.

$$\begin{aligned}\mathbb{I}_{1,1}(\Theta) &= \frac{1}{2\sigma_Y^2} N, \quad \mathbb{I}_{2,2}(\Theta) = \frac{Y_m^2}{2\sigma_Y^2} N \\ \mathbb{I}_{1,2}(\Theta) = \mathbb{I}_{2,1}(\Theta) = \mathbb{I}_{1,3}(\Theta) = \mathbb{I}_{3,1}(\Theta) &= 0 \\ \mathbb{I}_{2,3}(\Theta) = \mathbb{I}_{3,2}(\Theta) &= \frac{Y_m^2}{2\sigma_Y^2} \left(\frac{2\pi}{f_s}\right) \frac{N(N+1)}{2} \\ \mathbb{I}_{3,3}(\Theta) &= \frac{Y_m^2}{2\sigma_Y^2} \left(\frac{2\pi}{f_s}\right)^2 \frac{N(N+1)(2N+1)}{6}\end{aligned}\quad (24)$$

With $\mathbb{I}(\Theta)$ defined as in (24), various elements of its inverse, $\mathbb{I}^{-1}(\Theta)$, are obtained as follows.

$$\begin{aligned}\mathbb{I}_{1,1}^{-1}(\Theta) &= \frac{2\sigma_Y^2}{N}, \quad \mathbb{I}_{2,2}^{-1}(\Theta) = \frac{4\sigma_Y^2}{Y_m^2} \frac{(2N+1)}{N(N-1)} \\ \mathbb{I}_{1,2}^{-1}(\Theta) = \mathbb{I}_{2,1}^{-1}(\Theta) = \mathbb{I}_{1,3}^{-1}(\Theta) = \mathbb{I}_{3,1}^{-1}(\Theta) &= 0 \\ \mathbb{I}_{2,3}^{-1}(\Theta) = \mathbb{I}_{3,2}^{-1}(\Theta) &= \frac{-12\sigma_Y^2}{Y_m^2 N(N-1)} \frac{f_s}{2\pi} \\ \mathbb{I}_{3,3}^{-1}(\Theta) &= \frac{24\sigma_Y^2}{Y_m^2 N(N^2-1)} \left(\frac{f_s}{2\pi}\right)^2\end{aligned}\quad (25)$$

Finally, the CRBs for the variances of an estimator of Y_m , θ and f are given by $\mathbb{I}_{1,1}^{-1}(\Theta)$, $\mathbb{I}_{2,2}^{-1}(\Theta)$ and $\mathbb{I}_{3,3}^{-1}(\Theta)$ in (25), respectively, after substituting Y_m with its estimate \hat{Y}_m .

APPENDIX B

DERIVATION OF CRBS FOR SIGNAL PARAMETERS AFTER INCLUDING RoCoF IN THE ESTIMATION MODEL

After including RoCoF in (21), the estimation model is given as follows for $k = 1, 2, \dots, N$.

$$Y_k = Y_m \sin \phi_k + \epsilon_k, \quad \phi_k = \frac{2\pi k f}{f_s} + \frac{\pi k^2 R_f}{f_s^2} + \theta \quad (26)$$

The variance of the noise, denoted by ϵ_k , is σ_Y^2 . The new set of parameters which need to be estimated for (21) is $\Theta = \{\Theta_1, \Theta_2, \Theta_3, \Theta_4\} = \{Y_m, \theta, f, R_f\}$.

After evaluating the partial derivatives in (22) using (26), various elements of $\mathbb{I}(\Theta)$, besides those in (23), are as follows.

$$\begin{aligned}\mathbb{I}_{1,4}(\Theta) = \mathbb{I}_{4,1}(\Theta) &= \frac{Y_m}{2\sigma_Y^2} \sum_{k=1}^N \frac{\pi k^2}{f_s^2} \sin(2\phi_k) \\ \mathbb{I}_{2,4}(\Theta) = \mathbb{I}_{4,2}(\Theta) &= \frac{Y_m^2}{2\sigma_Y^2} \sum_{k=1}^N \frac{\pi k^2}{f_s^2} (1 + \cos(2\phi_k)) \\ \mathbb{I}_{3,4}(\Theta) = \mathbb{I}_{4,3}(\Theta) &= \frac{Y_m^2}{2\sigma_Y^2} \sum_{k=1}^N \frac{2\pi^2 k^3}{f_s^3} (1 + \cos(2\phi_k)) \\ \mathbb{I}_{4,4}(\Theta) &= \frac{Y_m^2}{2\sigma_Y^2} \sum_{k=1}^N \left(\frac{\pi k^2}{f_s^2}\right)^2 (1 + \cos(2\phi_k))\end{aligned}$$

where, $\phi_k = \frac{2\pi k f}{f_s} + \frac{\pi k^2 R_f}{f_s^2} + \theta$ (27)

Similarly, simplification of (27) gives the following expressions.

$$\begin{aligned}\mathbb{I}_{1,4}(\Theta) = \mathbb{I}_{4,1}(\Theta) &= 0 \\ \mathbb{I}_{2,4}(\Theta) = \mathbb{I}_{4,2}(\Theta) &= \frac{Y_m^2}{2\sigma_Y^2} \left(\frac{\pi}{f_s^2}\right) \frac{N(N+1)(2N+1)}{6} \\ \mathbb{I}_{3,4}(\Theta) = \mathbb{I}_{4,3}(\Theta) &= \frac{Y_m^2}{2\sigma_Y^2} \left(\frac{2\pi^2}{f_s^3}\right) \frac{N^2(N+1)^2}{4} \\ \mathbb{I}_{4,4}(\Theta) &= \left(\frac{\pi}{f_s^2}\right) \frac{3N^2+3N-1}{5} \mathbb{I}_{2,4}(\Theta)\end{aligned}\quad (28)$$

With $\mathbb{I}(\Theta)$ defined as in (24) and (28), the diagonal elements of its inverse, $\mathbb{I}^{-1}(\Theta)$, are obtained as follows.

$$\begin{aligned}\mathbb{I}_{1,1}^{-1}(\Theta) &= \frac{2\sigma_Y^2}{N}, \quad \mathbb{I}_{2,2}^{-1}(\Theta) = \frac{6\sigma_Y^2}{Y_m^2} \frac{(3N^2+3N+2)}{N(N-1)(N-2)} \\ \mathbb{I}_{3,3}^{-1}(\Theta) &= \frac{24\sigma_Y^2}{Y_m^2} \left(\frac{f_s}{2\pi}\right)^2 \frac{(2N+1)(8N+11)}{N(N^2-1)(N^2-4)} \\ \mathbb{I}_{4,4}^{-1}(\Theta) &= \frac{360\sigma_Y^2}{Y_m^2} \left(\frac{f_s^2}{\pi}\right)^2 \frac{1}{N(N^2-1)(N^2-4)}\end{aligned}\quad (29)$$

The CRBs for the variances of an estimator of Y_m , θ , f and R_f are given by $\mathbb{I}_{1,1}^{-1}(\Theta)$, $\mathbb{I}_{2,2}^{-1}(\Theta)$, $\mathbb{I}_{3,3}^{-1}(\Theta)$ and $\mathbb{I}_{4,4}^{-1}(\Theta)$ in (29), respectively, after substituting Y_m with its estimate \hat{Y}_m .

REFERENCES

- [1] National Grid, "Frequency change during large disturbances and their impact on the total system," Ind. Consultation Rep., Aug. 2013. [Online]. Available: <http://www2.nationalgrid.com/>
- [2] EirGrid and SONI, "Summary of studies on rate of change of frequency events on the all-island system," Tech. Rep., Aug. 2012. [Online]. Available: <http://www.eirgrid.com/>
- [3] K. Creighton, M. McClure, R. Skillen, J. O'Higgins, T. McCartan, and A. Rogers, "Increased wind generation in Ireland and Northern Ireland and the impact on rate of change of frequency," in *Proc. 12th Wind Integr. Workshop*, London, U.K., Oct. 22–24, 2013.
- [4] J. O'Sullivan, A. Rogers, D. Flynn, P. Smith, A. Mullane, and M. O'Malley, "Studying the maximum instantaneous non-synchronous generation in an island system—Frequency stability challenges in Ireland," *IEEE Trans. Power Syst.*, vol. 29, no. 6, pp. 2943–2951, Nov. 2014.
- [5] J. Xia, A. Dysko, and J. O'Reilly, "Future stability challenges for the UK network with high wind penetration levels," *IET Gener., Transmiss. Distrib.*, vol. 9, no. 11, pp. 1160–1167, Aug. 2015.
- [6] PPA Energy and TNEI, "Rate of change of frequency (ROCOF): Review of TSO and generator submissions," Final Rep., May 2013. [Online]. Available: <https://www.cru.ie/wp-content/uploads/2013/07/cer13143-appa-tnei-rocof-final-report.pdf>
- [7] F. Messina, P. Marchi, L. Rey Vega, C. G. Galarza, and H. Laiz, "A novel modular positive-sequence synchrophasor estimation algorithm for PMUs," *IEEE Trans. Instrum. Meas.*, vol. 66, no. 6, pp. 1164–1175, Jun. 2017.
- [8] L. Fu, J. Zhang, S. Xiong, Z. He, and R. Mai, "A modified dynamic synchrophasor estimation algorithm considering frequency deviation," *IEEE Trans. Smart Grid*, vol. 8, no. 2, pp. 640–650, Mar. 2017.
- [9] S. Maharjan, J. C. H. Peng, J. E. Martinez, W. Xiao, P. H. Huang, and J. L. Kirtley, "Improved sample value adjustment for synchrophasor estimation at off-nominal power system conditions," *IEEE Trans. Power Del.*, vol. 32, no. 1, pp. 33–44, Feb. 2017.
- [10] A. Shaik and P. Tripathy, "Development of phasor estimation algorithm for p-class PMU suitable in protection applications," *IEEE Trans. Smart Grid*, vol. 9, no. 2, pp. 1250–1260, Mar. 2018.
- [11] D. Macii, D. Fontanelli, G. Barchi, and D. Petri, "Impact of acquisition wideband noise on synchrophasor measurements: A design perspective," *IEEE Trans. Instrum. Meas.*, vol. 65, no. 10, pp. 2244–2253, Oct. 2016.
- [12] D. Fontanelli, D. Macii, and D. Petri, "Dynamic synchrophasor estimation using smoothed Kalman filtering," in *Proc. IEEE Int. Instrum. Meas. Technol. Conf.*, Taipei, Taiwan, May 23–26, 2016, pp. 1–6.
- [13] D. Belega, D. Fontanelli, and D. Petri, "Dynamic phasor and frequency measurements by an improved Taylor weighted least squares algorithm," *IEEE Trans. Instrum. Meas.*, vol. 64, no. 8, pp. 2165–2178, Aug. 2015.
- [14] J. A. de la O Serna, "Synchrophasor measurement with polynomial phase-locked-loop Taylor–Fourier filters," *IEEE Trans. Instrum. Meas.*, vol. 64, no. 2, pp. 328–337, Feb. 2015.
- [15] P. Romano and M. Paolone, "Enhanced interpolated-DFT for synchrophasor estimation in FPGAs: Theory, implementation, and validation of a PMU prototype," *IEEE Trans. Instrum. Meas.*, vol. 63, no. 12, pp. 2824–2836, Dec. 2014.
- [16] P. Castello, J. Liu, C. Muscas, P. A. Pegoraro, F. Ponci, and A. Monti, "A fast and accurate PMU algorithm for P+M class measurement of synchrophasor and frequency," *IEEE Trans. Instrum. Meas.*, vol. 63, no. 12, pp. 2837–2845, Dec. 2014.
- [17] D. Petri, D. Fontanelli, and D. Macii, "A frequency-domain algorithm for dynamic synchrophasor and frequency estimation," *IEEE Trans. Instrum. Meas.*, vol. 63, no. 10, pp. 2330–2340, Oct. 2014.
- [18] M. A. Platas-Garza and J. A. de la O Serna, "Dynamic phasor and frequency estimates through maximally flat differentiators," *IEEE Trans. Instrum. Meas.*, vol. 59, no. 7, pp. 1803–1811, Jul. 2010.
- [19] A. G. Phadke and J. S. Thorp, *Synchronized Phasor Measurements and Their Applications*. New York, NY, USA: Springer, 2008.
- [20] J. Borkowski, D. Kania, and J. Mroczka, "Interpolated-DFT-based fast and accurate frequency estimation for the control of power," *IEEE Trans. Ind. Electron.*, vol. 61, no. 12, pp. 7026–7034, Dec. 2014.
- [21] S. Julier, J. Uhlmann, and H. F. Durrant-Whyte, "A new method for the nonlinear transformation of means and covariances in filters and estimators," *IEEE Trans. Autom. Control*, vol. 45, no. 3, pp. 477–482, Mar. 2000.
- [22] S. M. Kay, *Fundamentals of Statistical Signal Processing: Estimation Theory*. Englewood Cliffs, NJ, USA: Prentice-Hall, 1993.
- [23] T. P. Zielinski and K. Duda, "Frequency and damping estimation methods—An overview," *Metrol. Meas. Syst.*, vol. 18, no. 4, pp. 505–528, Jan. 2011.
- [24] D. Belega and D. Dallet, "Frequency estimation via weighted multipoint interpolated DFT," *IET Sci., Meas. Technol.*, vol. 2, no. 1, pp. 1–8, Jan. 2008.
- [25] P. Kundur, *Power System Stability and Control*. Noida, India: McGraw-Hill, 1994.
- [26] P. Handel, "Properties of the IEEE-STD-1057 four-parameter sine wave fit algorithm," *IEEE Trans. Instrum. Meas.*, vol. 49, no. 6, pp. 1189–1193, Dec. 2000.
- [27] K. Ogata, *Modern Control Engineering*, 4th ed. Upper Saddle River, NJ, USA: Prentice-Hall, 2001.
- [28] A. K. Singh and B. C. Pal, "Decentralized dynamic state estimation in power systems using unscented transformation," *IEEE Trans. Power Syst.*, vol. 29, no. 2, pp. 794–804, Mar. 2014.
- [29] A. K. Singh and B. C. Pal, *Dynamic Estimation and Control of Power Systems*. New York, NY, USA: Academic Press, 2018.
- [30] B. Pal and B. Chaudhuri, *Robust Control in Power Systems*. New York, NY, USA: Springer, 2005.
- [31] A. K. Singh and B. C. Pal, "Report on the 68-bus, 16-machine, 5-area system," IEEE PES Task Force on Benchmark Systems for Stability Controls, version 3.3, Dec. 2013, pp. 1–41. [Online]. Available: <http://www.sel.eesc.usp.br/ieee/> or <https://eioc.pnnl.gov/benchmark/ieess/index.htm>
- [32] A. K. Singh, "Decentralized estimation and control for power systems," Doctoral dissertation, Dept. Elect. Electron. Eng., Imperial College London, London, U.K., 2014.
- [33] *IEEE Standard for Synchrophasor Measurements for Power Systems*, IEEE Standard C37.118.1-2011, Dec. 2011.
- [34] *IEEE Standard for Synchrophasor Measurements for Power Systems—Amendment 1: Modification of Selected Performance Requirements*, IEEE Standard C37.118.1a-2014 (Amendment to IEEE Standard C37.118.1-2011), Apr. 2014.
- [35] *IEEE Standard Requirements for Instrument Transformers*, IEEE Standard C57.13-2008 (Revision of IEEE Standard C57.13-1993), Jul. 28, 2008, pp. c1–c82.
- [36] *IEC Standard for Instrument Transformers*, IEC Standard 60044 ed. 1.2, 2003.



Abhinav Kumar Singh (S'12–M'15) received the B.Tech. degree from the Indian Institute of Technology Delhi, New Delhi, India, in 2010, and the Ph.D. degree from Imperial College London, London, U.K., in 2015, both in electrical engineering.

Since August 2017, he has been a Lecturer of power systems with the University of Lincoln, Lincoln, U.K. In April 2019, he will join the School of Electronics and Computer Science, University of Southampton, Southampton, U.K. He has also been a Visiting Researcher with Imperial College London

since September 2017. His research interests include estimation, control, and communication aspects of power systems with significant integration of renewable sources of energy.



Bikash C. Pal (M'00–SM'02–F'13) received the B.E.E. (Hons.) degree from Jadavpur University, Kolkata, India, in 1990, the M.E. degree from the Indian Institute of Science, Bangalore, India, in 1992, and the Ph.D. degree from Imperial College London, London, U.K., in 1999, all in electrical engineering.

He is currently a Professor with the Department of Electrical and Electronic Engineering, Imperial College London. His research interests include state estimation and power system dynamics.

Dr. Pal was an Editor-in-Chief of the IEEE TRANSACTIONS ON SUSTAINABLE ENERGY.